Oil trajectory analysis for oil spill surveillance by SAR in the Mediterranean Sea

Article *in* Marine Pollution Bulletin · March 2023

DOI: 10.1016/j.marpolbul.2023.114825

1 author:

Achille Ciappa
e-GEOS

31 PUBLICATIONS **411** CITATIONS

SEE PROFILE

Title: Oil trajectory analysis for oil spill surveillance by SAR in the Mediterranean Sea.
Author: Achille Carlo Ciappa

DRAFT VERSION

ABSTRACT

Oil trajectory analysis (OTA) provides statistics of direction and distance of provenience of oil spills reaching specific coastal sites. Applied to marine protected areas (MPA), this information could be used to introduce priority criteria in satellite oil spill surveillance. OTA in the Mediterranean Sea was based on 10-days oil trajectories tracked backward-in-time for five years (2015-2019) and aggregated on monthly basis. On average, travel time increases from 12h at 5 km from the coast to 1.5 days at 10 km and 2 days at 15 km. The beaching probability decreases from 25% at 5 km to 8% at 10 km and 5% at 15 km. Locally, the oil transport is influenced by persistent winds and/or energetic current systems in the area. Using an attention threshold of 5% of beaching probability around MPA, several offshore areas of the Mediterranean Sea deserving high monitoring priority in summer and winter have been identified.

1 - Introduction

Oil slicks on the sea surface are detected in X- and C-band Synthetic Aperture Radar (SAR) images independently of clouds and for a wide wind speed range (too low and too high speeds are excluded). SAR images are traditionally acquired by large and expensive satellites owned by institutional space agencies (as X-band TerraSAR, COSMO-SkyMed and KOMPSAT-5, C-band RADARSAT and Copernicus Sentinel-1), but many private operators of 'small satellites' constellations have recently appeared (X-band Finland's Iceye, U.S. Capella Space, Sequoia, PredaSAR and Umbra, Japan's iQPS , C-band Chinese Hisea-1, Gaofen-3). In the near future, a growing number of SAR images will be available for oil spill detection. Oil spill surveillance will benefit as a matter of course from a more significant amount of data, but it will still be necessary to establish priority criteria to decide where specifically to acquire more data or how to specifically process the increased amount.

It is certainly useful to monitor sea areas where oil spills most frequently occurred in the past. Organizations maintaining these databases are the Regional Marine Pollution Emergency Response (REMPEC), gathering data since 1977 (Carpenter et al., 2017), the International Tanker Owners Pollution Federation Limited (ITOPF), which provides data on oil spills from tankers since 1970 (ITOPF Handbook 2022), and the CleanSeaNet satellite observation service of the European Maritime Satellite Agency (EMSA), gathering data on oil spills detected by SAR since 2007. In the case of CleanSeaNet service, SAR satellite data tasking (the request of new acquisitions) is carried out by EMSA in cooperation with member states to meet their service coverage requirements (Carpenter et al., 2016). A different strategy could be adopted by the various states surrounding the Mediterranean Sea. Recent statistics of oil spills in the Mediterranean Sea are discussed in Polinov et al. (2021), illustrating the need to understand the

spatial-temporal patterns of oil spills. Provenance spots with a higher disruptive potential deserve special consideration, i.e. sea areas from which oil spills have some probability of reaching one or more marine protected areas or coastal areas of peculiar interest.

This information is provided in this study by the oil trajectory analysis of 10-days trajectories simulated for five years in the Mediterranean Sea (2015-2019). Oil trajectory analysis is based on trajectories tracked backward-in-time, i.e. starting from thousands of beaching sites on the coast and ending 10 days before offshore. The backtracking method is commonly used in tracing the pollutants' origin and has been adopted in several oil spill studies (Abascal et al., 2012; Janeiro et al, 2017; Thyng, 2019; Chen, 2019). The trajectories, for a total of $3.1* 10^8$ released in 5 years, have been aggregated on a month-by-month basis, extracting information on the location of the oil spill and the probability and time necessary for it to reach a specific coastal site. Finally, this information was applied to the marine protected areas of the Mediterranean Sea. Details on the simulations, run organization, data be stored during the simulations and a validation case with a real oil spill are described in Section 2. Section 3 illustrates results obtained at basin scale and in macro-areas where many protected areas are concentrated. Methodology and results are discussed in Section 4, also illustrating guidelines for oil trajectory analysis and its practical use in oil spill surveillance by SAR. Final conclusions are drawn in Section 5.

2 - Materials and methods

Oil trajectory analysis provides statistics of direction and distance of provenience of oil spills reaching specific coastal sites. In this study, oil trajectory analysis in the Mediterranean Sea was based on 10-days oil trajectories tracked backward-in-time for five years (2015-2019) and aggregated on monthly basis. This information applied to marine protected areas has been used to introduce priority criteria in satellite oil spill surveillance.

2.1 – Used data

Oil is advected by the surface current and by the wind. The surface current fields have been extracted from the Copernicus Marine Environmental Service (CMEMS) dataset MEDSEA_MULTIYEAR_PHY_006_004 (doi: 10.25423/CMCC/MEDSEA_MULTIYEAR_PHY_006_004_E3R1), a re-analysis product at 0.042° spatial resolution (around 4-5 km) where hourly and daily data at several depths are available (Escudier et al., 2020). Wind data have been extracted from the CMEMS product WIND_GLO_PHY_L4_MY_012_006 (doi: 10.48670/moi-00185), which merges ECMWF ERA5 re-analysis and scatterometer data, providing hourly wind fields at 0.125° spatial resolution (around 12-14 km). Daily surface currents and 6-hours winds from 2015 to 2019 have been used in the simulations. Fig. 1 shows an example of surface current on 30th June 2018 and wind at 12:00, one of the four wind fields used per day.

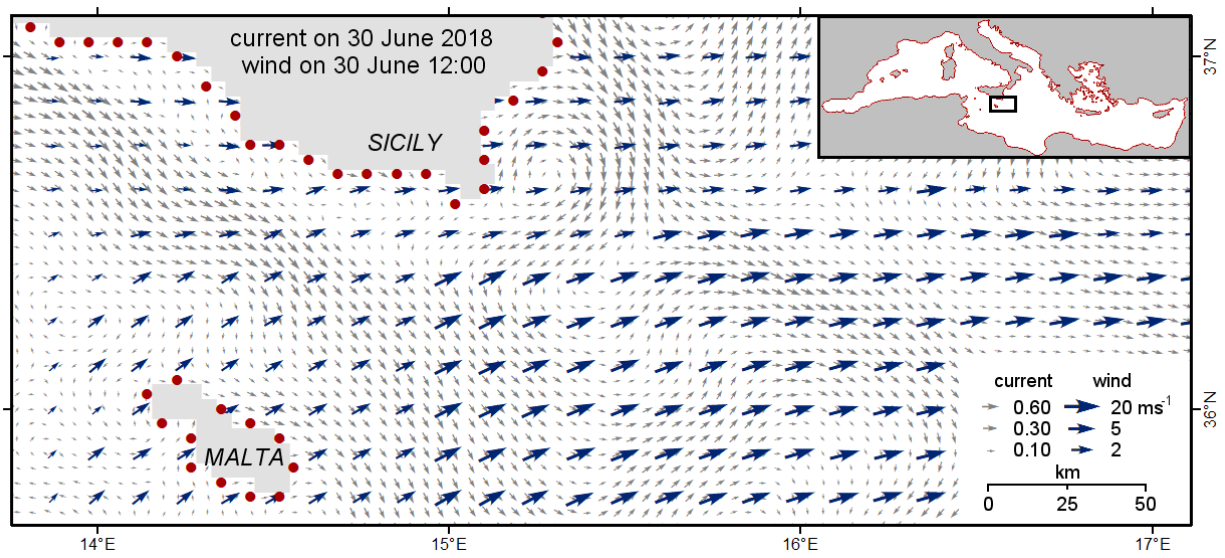

Fig.1 - Sea surface current and wind field south of Sicily on 30 June 2018 (wind at 12:00). The spatial resolution is 0.042° for current, 0.125° for wind. The coastline consists of 2677 beaching sites (in red) used in the simulations.

2.2 – Simulations and run organization

Oil trajectories have been simulated backward-in-time, starting from the coast (beaching sites) and spreading offshore for 10 days before. The trajectories start from 2677 points spaced around 8-9 km along the coast (red dots in Fig.1, mean distance 8.3 km), which are the beaching sites. The beaching sites are source of trajectories in reverse modelling and will be referred to as 'sources'.

The oil transport equation includes the advection of the surface current and of the wind, the latter commonly estimated to be 3% of the wind speed (ASCE, 1996), and a diffusion term simulated by random walk:

$$x_{t-1} = x_t - \vec{\boldsymbol{u}}_{curr}\Delta t - 0.03 \cdot \vec{\boldsymbol{u}}_{wind}\Delta t + \overrightarrow{\boldsymbol{rand}} \cdot \sqrt{2k_h/\Delta t} \cdot \Delta t$$

with $\overrightarrow{rand}$ as random unitary vector. About the use of random walk in backtracking, Flesch et al. (1995) found that the correspondence between forward and backward models is good in the case of turbulent diffusion notwithstanding the irreversibility of the process, on condition that any sort of deterministic bias to the direction of motion arising from turbulence non-homogeneity is considered (''well-mixed'' condition, in Thomson, 1987). As random walk is commonly used to simulate the physical process of turbulent diffusion in the forward mode; random walk in the backward mode describes the uncertainty of the trajectory caused by turbulent diffusion and the result of backward-in-time integration provides probabilities of possible source locations. In OTA the oil is treated as passive particles and the "weathering" process is not included. Weathering includes a wide variety of physical, chemical, and biological processes that begin to transform the oil almost immediately after its release (Fingas, 2011): over 70% of a heavy fuel spill persists for a week or longer, and over 90% of a diesel spill is either evaporated or naturally dispersed into the water column in time frames of a couple of hours to a couple of days. In OTA, weathering is not included because the type of oil that could be spilled is not known; moreover, it is not

relevant if part of the oil evaporates: what really matter is if the oil, or traces of oil reach the beach. The motion equation used here is the same adopted in recent similar studies (Abascal et al., 2012; Ciappa and Costabile, 2014; Suneel et al., 2016; Janeiro et al, 2017; Chen, 2019; Ciappa, 2021).
Each trajectory was simulated for 10 days with a time step of 30 min, and current and wind data have been linearly interpolated at time and position of each trajectory. The trajectories that beached before of 10 days have been used only from the source to the beaching site. The adopted diffusion coefficient is $k_h = 5\,m^2/s$ (Viikmäe et al., 2013). With this assumption, oil from a perpetual source spreads in a circle of 5 km radius in 10 days (not shown). Runs were organized on a monthly basis and trajectories were simulated for the same month over a five-year period (2015 – 2019). Each monthly run was extended for a further 10 days, as the beaching events at the beginning of the month are due to trajectories of the previous month. One trajectory per time step was released from every source point (2677), for an average of $2.5*10^7$ trajectories released per month.

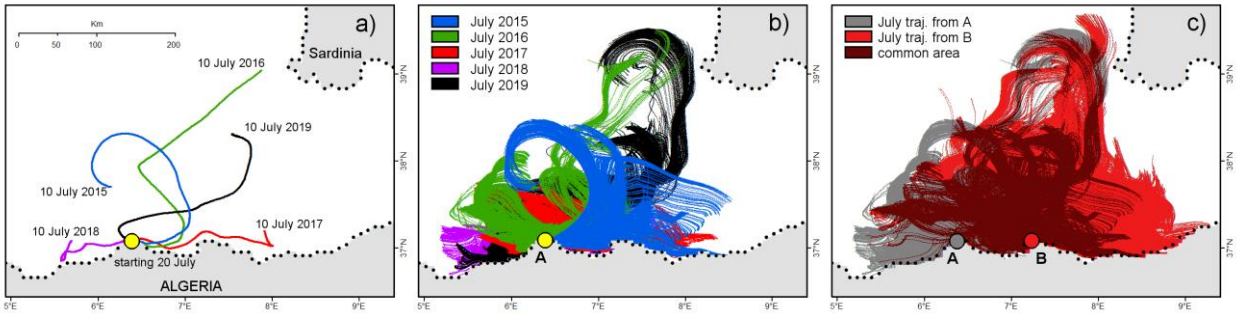

Fig. 2a. Five trajectories starting from a coastal site on the Algerian coast on 20 July 00:00 and tracked backward-in-time until 10 July 00:00 in years 2015-2019. Fig. 2b. All the trajectories (9840) released in July 2015 – 2019 from source point A. Fig. 2c. All the trajectories in July from source points A and B and common sea area.

Fig. 2a illustrates the five trajectories from a source point on the Algerian coast tracked backward-in-time from 20 July 00:00 to 10 July 00:00 of different years. Fig. 2b illustrates the trajectories released from 2015 to 2019 in A in July. Fig. 2c shows what happens when trajectories from two sources are combined: the common area (in dark red) is crossed by trajectories from A and B, meaning that an oil spill detected there has some probability to reach point A and point B. The frequent loops are due to the formation of eddies in this sector of the Algerian Current (Millot, 1999).

2.3 – Stored data and final maps

Month by month, all the trajectories have been reported on a regular grid, shown in Fig. 3. For convenience, the chosen grid is the same of current data (0.042°). In each grid cell, the crossing trajectories coming from many sources have been counted and separated by 'source' of provenience. As an example, Fig. 3a shows the grid point G off the northern coast of Crete in July and Table 1 shows the data stored in

G. Trajectories crossing G come from 17 sources (s1 - s17 in Fig. 3a) and a number of crossing trajectories, minimum and average travel time have been stored for each source (Table 1). The beaching probability of G in these 17 sources is the ratio of the crossing trajectories by the total number of trajectories released by the source over the month (9840 for July). The beaching probabilities (Table 1) are 11.6 % in s7, followed by s6 (11.3 %) and s8 (9.2 %). This means that an oil spill detected in G in July will most likely beach in s7 (11.6%), followed by s6 and s8.

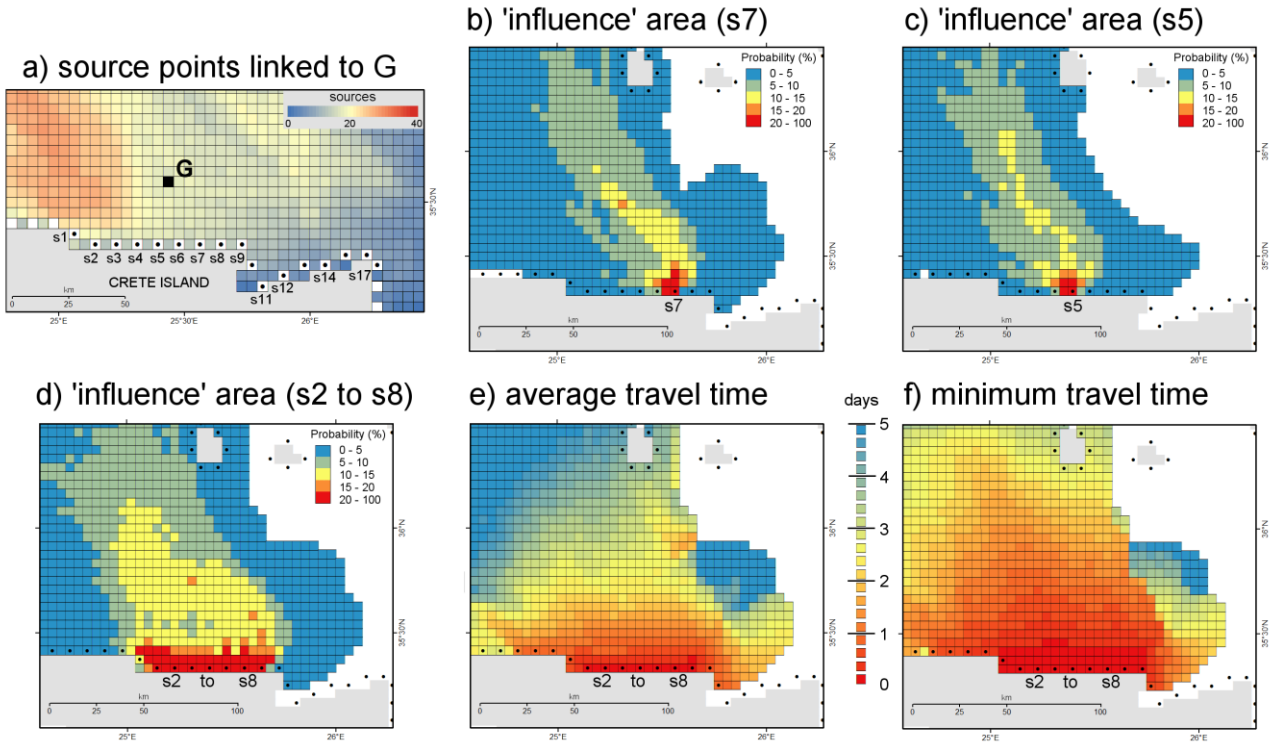

Fig. 3a. Number of sources (beaching sites) per grid cell in July north of Crete Island. Grid cell G is linked to 17 sources on the coast (s1 to s17), and the highest beaching probability occurs in s7 (11.6%). Fig. 3b. 'Influence' area of source s7, i.e., from where oil spills can reach s7 in July. Fig. 3c. Influence area of source s5. Fig. 3d. Influence area of the hypothetical marine protected area s2 to s8. Fig. 3e. Average travel time. Fig. 3f. Minimum travel time.

Table 1 – Parameters extracted in the grid cell G in Fig. 3a. Sources s1 to s17 are reported from west to east.

POINT G	Number of sources = 17																
Source	s1	s2	s3	s4	s5	s6	**s7**	s8	s9	s10	s11	s12	s13	s14	s15	s16	s17
Crossing trajectories	46	38	186	512	859	1113	**1145**	906	417	106	74	235	331	320	166	202	115
Min travel time (days)	4.3	4.1	1.3	1.0	0.9	0.8	**0.7**	0.8	1.0	1.6	1.9	1.6	1.6	1.7	1.9	2.1	2.2
Ave travel time (days)	4.5	4.5	2.2	2.2	1.9	1.7	**1.6**	2.1	2.2	4.0	3.1	2.9	3.2	3.5	3.7	3.9	3.8
Probability (%)	0.5	0.4	1.9	5.2	8.7	11.3	**11.6**	9.2	4.2	1.1	0.7	2.4	3.4	3.2	1.7	2.0	1.2

The data stored in Table 1 link each sea grid cell (as G) to a number of coastal locations (as s1-s17) and vice versa. For instance, an oil spill in G will beach from s1 to s17, most likely in s7 (Fig. 3a). Similarly, the 'influence' zone of s7, i.e., all the grid points offshore from where an oil spill could reach s7 in July, can be easily extracted (Fig. 3b), and the same for source s5 (Fig. 3c). If s2 to s8 are merged, as in the case of hypothetical marine protected area, the influence area is obtained merging the highest probability of single-source maps (Fig. 3d). Average (Fig. 3e)

and minimum (Fig. 3f) travel time are the other extracted parameters. In this case, travel times are shorter than usual due to the northern 'meltemi' wind blowing in summer in south Aegean.

The only adopted measure during the runs was to store the data when the trajectory crosses the grid cell for the first time. Actually the same trajectory could cross the same cell many times if looping or going back and forward. The latter eventuality was taken into account storing the previous path of the trajectory during the run.

2.4 – Validation with a real oil spill

Oil trajectory analysis provide statistics of direction and arrival time (up to 10 days, in this case) of oil spills on the coast basing on oil trajectories tracked backward-in-time. It was verified that oil trajectory analysis includes the evolution of a real oil spill, as the oil spill occurred off the northern coast of Corsica on 7th October 2018. After the accident, the oil spill was detected by Sentinel-1B on 8th October (Fig. 4a) and by Sentinel-1A on 13th October, five days later (Fig. 4b). The oil beached from 16 to 25 of October on the French coast from Frejus to Tolon (Fig. 4a), then reached the Spanish coast in November. The emergency operations are reported in Soussi et al. (2019) and Liubartseva et al. (2020).

Oil trajectory analysis, applied to the oil detected in the first SAR image on October 8th, indicates as beaching sites the northern coast of Corsica, an extended sector of the Italian coast from Genoa to Mentone and the French coast south of Frejus (Fig. 4a). The true beaching sites are included in the list. The other points along the northern Italian coast and on the northern coast of Corsica, the latter very close to the spill, are due to the possibility of northern and southern transport patterns in October. In the following 5 days, the oil drifted about 100 km to NNW and fragmented in several slicks, as shown in Fig. 4b. In this position, the oil was within the influence area of the Northern Current flowing westwards from the Italian to the French coast. From this new position, except for a few beaching sites between Imperia and Cannes, the predicted beaching sites (Fig. 4b) and relative arrival times (Fig, 4c) agree with the oil beached on French coast reported from 16 to 25 of October. This case shows that the results of oil transport analysis include the evolution of the Corsica oil spill in October 2018.

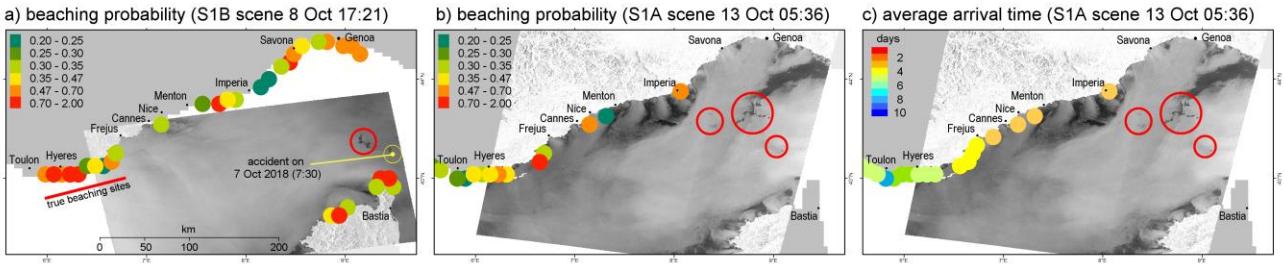

Fig. 4a. The oil spill occurred off the northern coast of Corsica (on 7 October at 7:30, in yellow) detected by Sentinel-1B on 8/10/2018 at 17:21 and relative beaching probability. Fig. 4b. The oil spill detected by Sentinel-1A on 13/10/2018 fragmented in three sections (in red) and relative beaching probability. Fig. 4c. Average arrival time of the slicks detected on 13/10/2018.

3 - Results

3.1 - General results

Oil trajectory analysis provides statistics of direction and arrival time (up to 10 days, in this case) of oil spills on the coast. 10-days trajectories cover all the coastal and most of the offshore area: 70.3% of the Mediterranean surface was crossed all year long by 10-days trajectories and only 3.1% was never crossed. The covered area is larger in winter than in summer, with a covering of over 90% from December to March and less than 85% from May to September, and the minimum (79%) in August. Fig. 5 shows four monthly probability maps (maximum beaching probability per grid cell). The two winter (Fig. 5a and Fig. 5b) and two summer maps (Fig. 5c and Fig. 5d) are similar, the sign of two marked seasons. Table 2 reports the correlations of the monthly probability maps, similar in summer (May to September) and in winter (November to March).

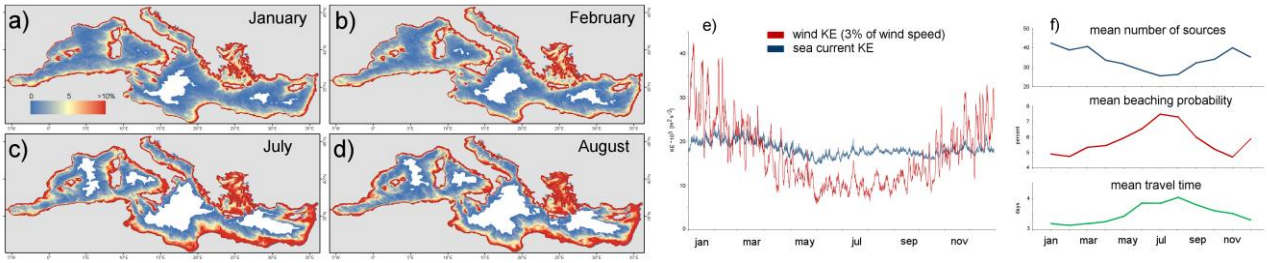

Fig. 5a-d. Monthly probability maps (maximum beaching probability per grid cell) in winter (Fig. 5a and Fig. 5b) and in summer (Fig. 5c and Fig. 5d). White areas are sea areas from where an oil spill takes more than 10 days to reach the coast. Fig. 5e. Kinetic energy of current and wind advection (3% of the wind speed). Fig. 5f. Monthly number of sources, probability, and minimum travel time per grid cell.

Table 2 – Correlations of monthly probability maps. Probability maps from May to September and from November to March are similar (correlations higher than 0.90). The lowest correlations are between July or August and January or November.

	May	Jun	Jul	Aug	Sep	Oct	Nov	Dec	Jan	Feb	Mar	Apr
May	1.00	**0.94**	0.88	0.86	**0.92**	0.89	0.86	0.87	0.85	0.88	0.89	**0.94**
Jun		1.00	**0.94**	**0.92**	**0.93**	0.87	0.79	0.84	0.78	0.81	0.82	0.89
Jul			1.00	**0.94**	**0.91**	0.84	0.74	0.81	0.73	0.76	0.76	0.83
Aug				1.00	**0.93**	0.87	0.75	0.83	0.73	0.77	0.76	0.83
Sep					1.00	**0.93**	0.83	0.87	0.81	0.84	0.84	0.89
Oct						1.00	**0.90**	**0.92**	0.85	0.88	0.86	**0.91**
Nov							1.00	**0.91**	**0.93**	**0.94**	**0.91**	**0.90**
Dec								1.00	**0.91**	**0.92**	0.88	0.89
Jan									1.00	**0.95**	**0.96**	**0.90**
Feb										1.00	**0.93**	**0.91**
Mar											1.00	**0.94**
Apr												1.00

The seasonal change is due to the dominance of the current on the wind advection, shown in terms of kinetic energy in Fig. 5e. Oil trajectories are mainly driven by the current in summer and by the wind in winter. As a

consequence, in summer the number of sources (beaching sites) is smaller and beaching probability and travel time are higher than in winter (Fig. 5f). The oil transport in summer is less energetic (longer travel time) and less chaotic (higher beaching probability) than in winter, and in winter, pushed by the wind, the oil reaches more beaching sites (but with a lower probability). This is the mean scenario in the Mediterranean Sea, but the local oil transport is influenced by persistent winds and current systems in the area, as discussed in Section 4. Appendix A reports separate maps of current and wind kinetic energy month by month, evidencing the main currents and local winds.

On average, travel time increases from 12h at 5 km from the coast to 1.5 days at 10 km and 2 days at 15 km; the beaching probability decreases from 25% at 5 km to 8% at 10 km and 5% at 15 km. The sea areas where the oil spill surveillance should be focused have been selected using an attention threshold of 5% of beaching probability in marine protected areas.

3.2 – Oil trajectory analysis in local sea areas

Fig. 6 shows the main protected areas of the Mediterranean Sea (source MAPAMED, the database of MArine Protected Areas in the MEDiterranean, 2019 edition, version 2, © 2022 by SPA/RAC and MedPAN, licensed under CC BY-NC-SA 4.0), and the main tanker routes (source European Marine Observation and Data Network (EMODnet): EMSA tanker route density map of 2019). As most of oil spills occur along the tanker routes (Jimenez Madrid et al., 2016; Polinov et al., 2021), five areas (A1 – A5), critical for the vicinity of marine protected areas to the main tanker routes, and three other areas (B1 – B3), critical for the vicinity of main tanker routes to the coast, have been investigated. Other critical areas meriting future investigation for the intense traffic are south of Sardinia, east of Sicily, south of Peloponnese (22°E), and south of Crete.

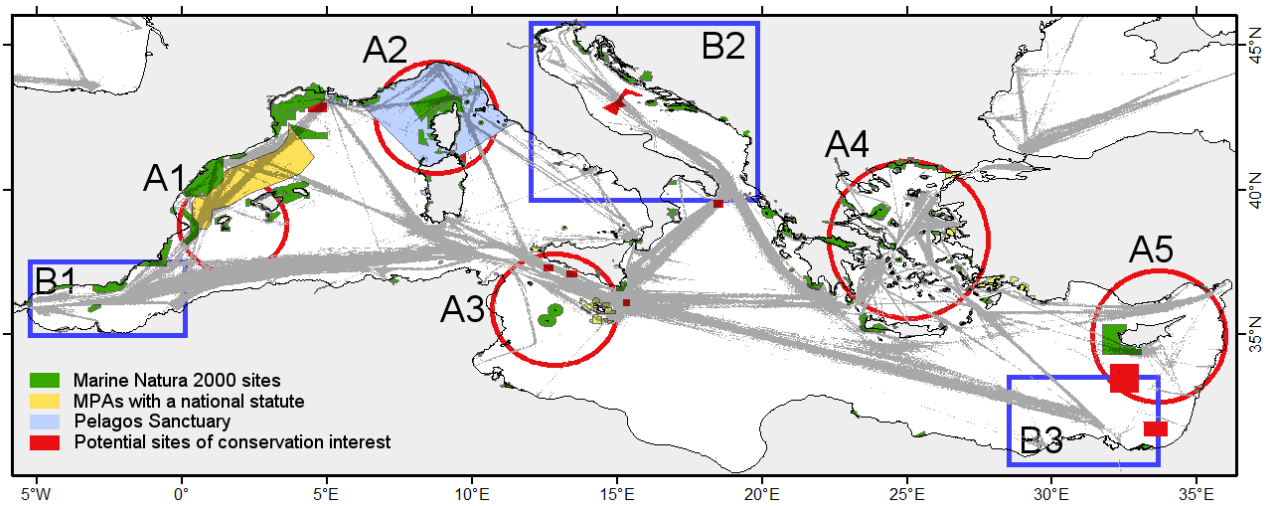

Fig. 6. Main protected areas (source: MArine Protected Areas in the MEDiterranean, (MAPAMED)) and tanker routes during 2019 (EMODnet 'sea route density' AIS data). A1 to A5 are areas where the tanker routes are close to marine protected areas, B1 to B3 are areas where the tanker routes are close to the coast.

A1 – West Med around Balearics

The red 'sources' in Fig. 7a are the beaching sites of the protected areas. Along the Valenciana coast (Alicante – Cartagena) in August (Fig. 7b) and west of Balearics in December (Fig. 7c) the area of beaching probability > 5% is intersected by the tanker routes, which is critical based on the premises of this study. The offshore extension of the 5% probability area between Alicante and Cartagena in summer (Fig. 7b) is probably due to summer sea breeze (Azorin-Molina at al., 2011), west of Balearics to the combination of winter winds and the Balearic Current (Garcia et al., 1994). These scenarios do not change from April to September (Fig. 7b) and from November to February (Fig. 7c).

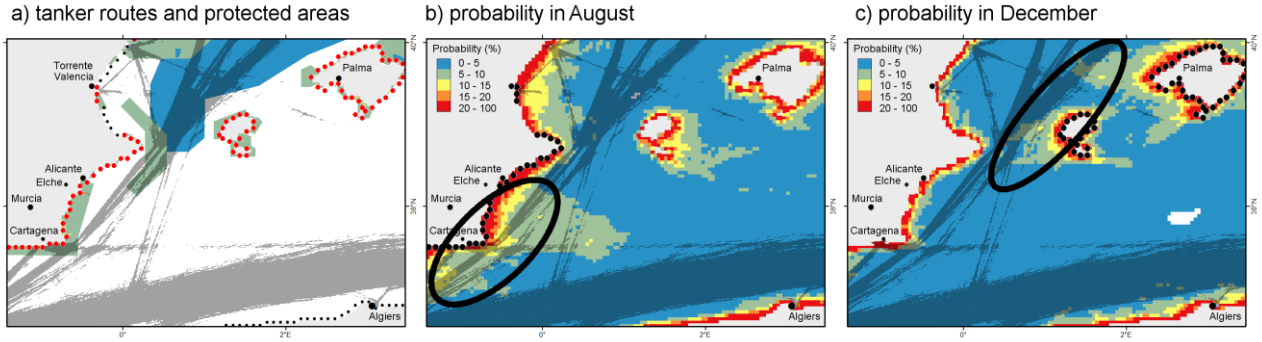

Fig. 7a. Main tanker routes and protected areas in West Mediterranean around Balearics. The marine protected areas are indicated by the red dots along the coast. Fig. 7b. Probability map (August) showing the extent of the 5% probability area from Alicante to Cartagena in summer. Fig. 7c. Probability map (December) showing the extent of the 5% probability area west of Balearic Islands in winter.

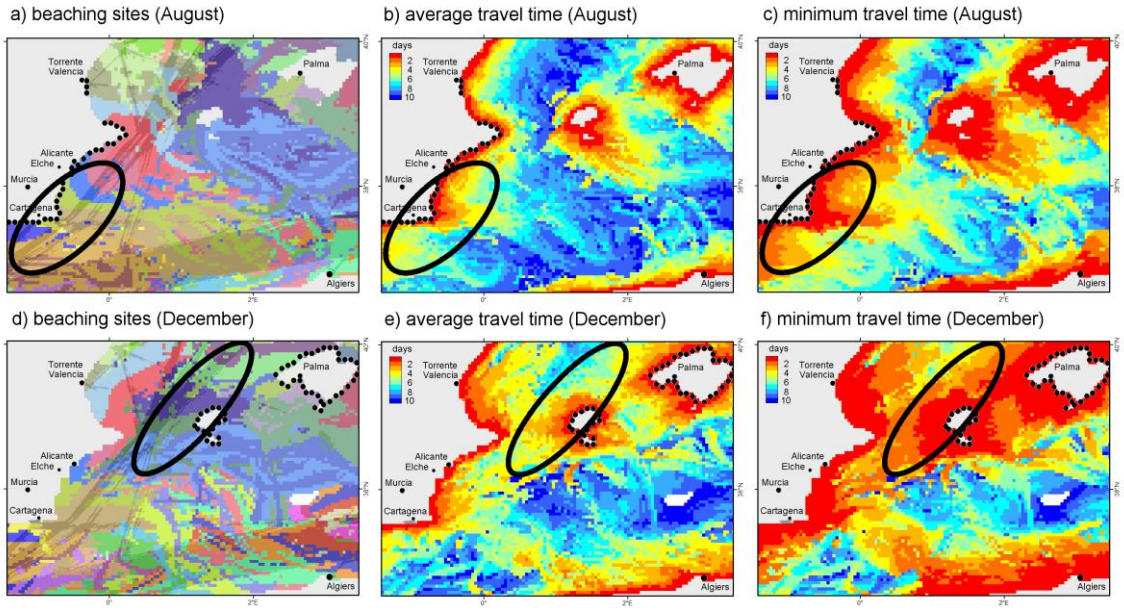

Fig. 8a and Fig. 8d. Beaching site maps indicating the most probable beaching sites distinguished by colour (10 beaching sites per colour) in summer (Fig. 8a) and in winter (Fig. 8d). Fig. 8b and Fig. 8e. Average travel time. Fig. 8c and Fig. 8f. Minimum travel time.

Fig. 8 shows other maps that can be extracted from the results of oil trajectory analysis. The beaching site maps (Fig. 8a and Fig. 8d) report the most likely

beaching site, using the same colour for sea areas and relative beaching sites (10 beaching sites per colour). Fig. 8a shows that the coast between Alicante and Cartagena in summer is most likely reached by oil spills from SE, and Fig. 8d shows that the western coast of Balearics in winter is most likely reached by oil spills from west. The average travel time from the tanker route east of Cartagena in August (Fig. 8b) is less than 3 days, 5-6 days west of Balearics in December (Fig. 8e). The minimum travel time is on average 1 day shorter (Fig. 8c and Fig. 8f).

A2 and A3 - North Tyrrhenian and Tuscany Islands, Sicily Channel and islands

North Tyrrhenian includes the Pelagos sanctuary (in cyan, in Fig. 9a) and many protected areas along the coast. In this area most of the tanker traffic does not involve crude oil (Jiménez Madrid et al., 2016). In the Strait of Bonifacio (Fig. 9b), the beaching probability increases from May to July with a peak in July (Fig. 9c). In the Gulf of Genoa, the beaching probability increases in summer between La Spezia and Genoa (Fig. 9c). Between Corsica and Tuscany Islands, the tanker traffic is intense all year round and the area east of Corsica is more critical in winter (Fig. 9b). In the Sicily Channel (Fig. 9d), tanker routes are concentrated between Sicily and Malta. The high probability areas north-west of Pantelleria and Malta (Fig. 9e and Fig. 9f) are due to stable surface current patterns (Atlantic Ionian Stream (AIS) in summer, in Astraldi et al., 1996; 1998; Robinson et al., 1999) and are intersected by the main tanker route. Another high risk area is at the westernmost tip of Sicily in winter (Fig. 9e), around the Egadi marine protected area (Ciappa and Costabile, 2014).

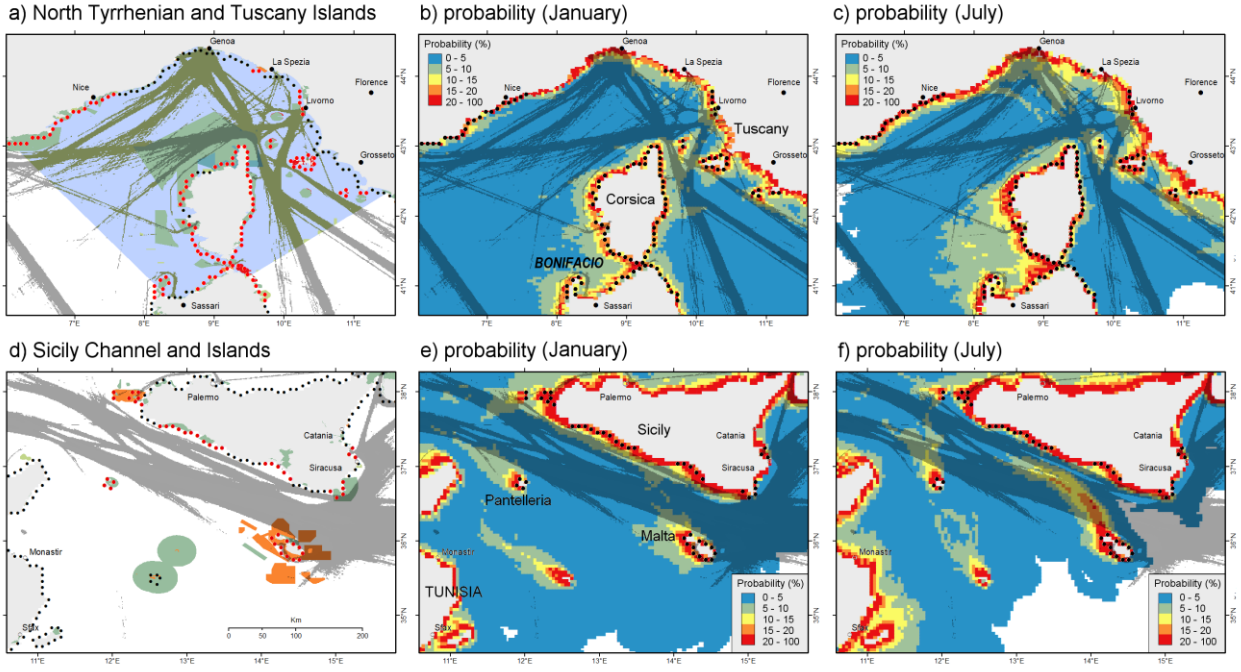

Fig. 9a and Fig. 9d. Main tanker routes and protected areas in North Tyrrhenian and Sicily Channel (protected areas are indicated by the red dots). Fig. 9b and Fig. 9e. Probability maps in January. Fig. 9c and Fig. 9f. Probability maps in July.

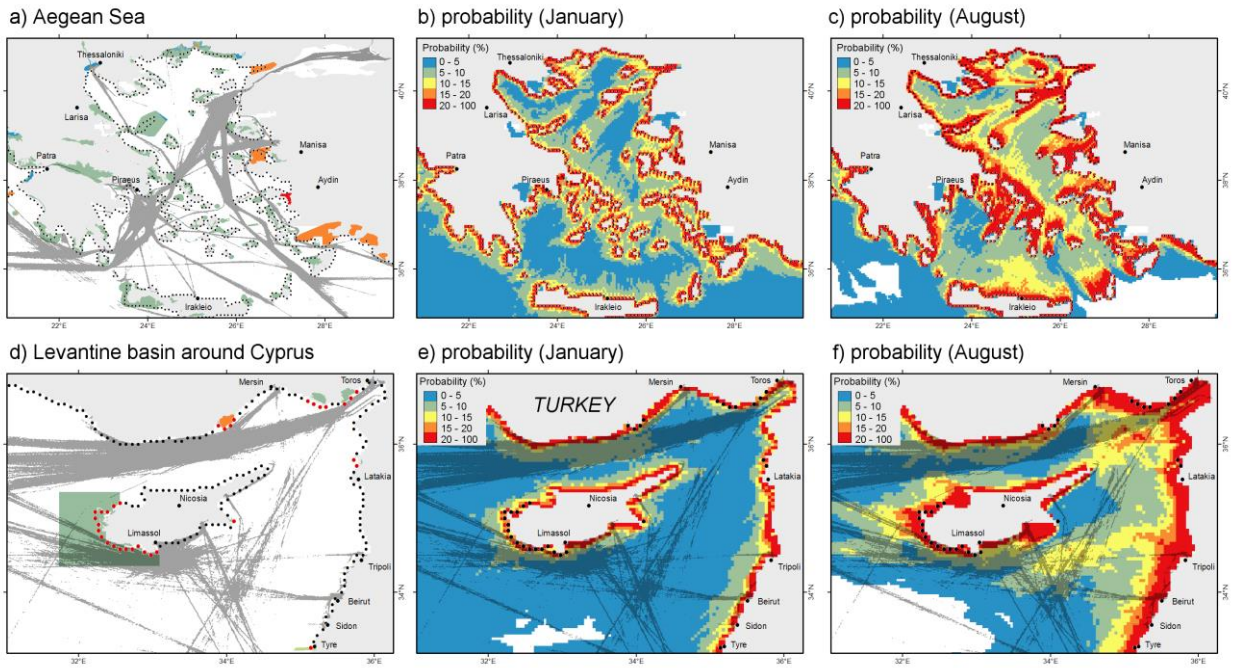

Fig. 10a and Fig. 10d. Main tanker routes and protected areas in Aegean Sea and around Cyprus (protected areas are indicated by the red dots). Fig. 10b and Fig. 10e. Probability maps in January. Fig. 10c and Fig. 10f. Probability maps in August.

A4 and A5 - Aegean Sea and Levantine basin around Cyprus

The intense tanker traffic in the Aegean Sea puts many protected areas at risk (Fig. 10a). The beaching probability is more than 10% in 35% of the Aegean surface in winter (Fig. 10b) and in 55% of the Aegean surface in summer (Fig. 10c). The most critical period is summer due to northern 'meltemi' wind. The straits through the islands are critical, especially through Cyclades (Ciappa, 2021). Cyclades would be more protected if the western tanker route to Black Sea (Fig. 10a) were shifted eastwards to overlap the eastern route, with an additional path of 200 nm.

In the Levantine basin (Fig. 10d), the tanker route is very close to the southern Turkish coast and the critical period is winter (Fig. 10e). Oil spills in this area drift westwards pushed by the Asia Minor Current (AMC). Probability increases along the eastern Mediterranean coast in summer (Syria, Lebanon, Israel, in Fig. 10f), as reported in Zodiatis et al. (2017a). The probability west and south Cyprus is higher in summer (May-September, Fig. 10f). An extensive analysis of the oil spill risk in the area is provided in Alves et al. (2015).

Other critical areas (B1 – B3)

Three other critical areas where tanker routes are close to the coast are shown in Fig. 11. The Spanish coast in the Alboran Sea (Fig. 11a) is a 'hotspot' of past incidents (Jiménez Madrid et al., 2016). In the Adriatic Sea (Fig. 11b), the northern part of the basin and the southern coast are critical in summer, as outlined in Liubartseva et al. (2014). The coastal area of the Eastern Mediterranean is especially critical in summer (Fig. 11c), and the region includes many offshore platforms (Zodiatis et al., 2017a).

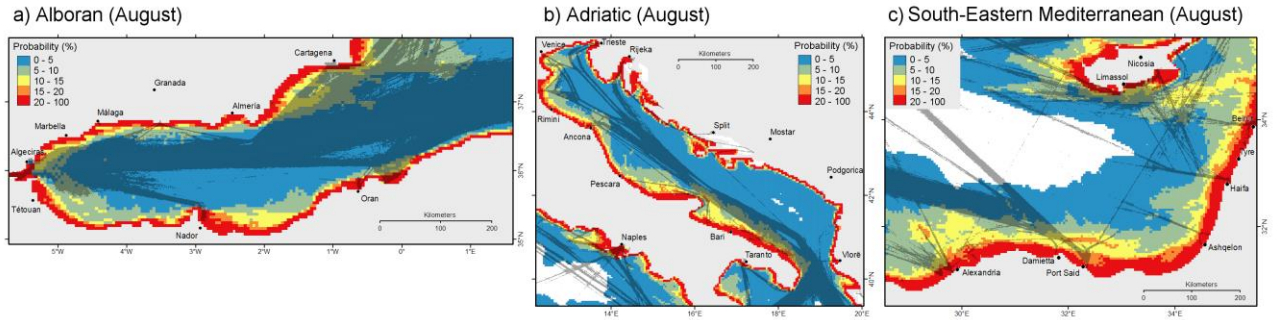

Fig. 11. Probability maps in August in the Alboran Sea (Fig. 11a), in the Adriatic Sea (Fig. 11b) and in south-eastern Levantine (Fig. 11c).

4 - Discussion

Oil trajectory analysis is a pioneering concept of oil spill modelling developed by the Hazardous Material Response Branch (HAZMAT) of National Oceanic and Atmospheric Administration (NOAA) (Torgrimson, 1981; Galt and Payton, 1983). In the receptor mode of the On Scene Spill Model (OSSM), used since the Exxon-Valdez oil spill, oil trajectories were back-tracked from one single point on the coast using wind statistics and the mean surface current. Today, detailed current and wind data provide more reliable results of oil trajectory analysis than in the past.

The basic features of oil trajectory analysis are: (i) a large number of coastal points representing the beaching sites, (ii) the discretization of the sea area, i.e. sea grid cells over a regular grid, and (iii) the link between the two geographical datasets, consisting of a large number of oil trajectories simulated by the Euler's motion equation. All these features can be improved: (i) more beaching sites along the coast; (ii) a finer spatial resolution grid where the results of the simulations are aggregated; (iii) winds and currents at finer time and spatial resolution, and (iv) refinements of the motion equation, as an advanced parametrization of advection and diffusion terms (Sbragio and Martins, 2022) and the introduction of sea roughness (De Dominicis et al., 2016). A useful option is to track the trajectories backward-in-time rather than forward-in-time. Indeed, backward-in-time integration is more computationally efficient when the number of receptors (destinations) is significantly lower than the number of potential sources (Batchelder, 2006). If forward-in-time integration had been used in this study, trajectories would have been released from all the sea grid cells (around $1.5*10^5$), instead of only the 2677 sources actually employed.

Lagrangian trajectories have been used to simulate the oil drift in the Baltic Sea and in the Gulf of Finland (Murawski and Woge Nielsen, 2013, Soomere et al., 2010; Lu et al., 2012; Delpeche-Ellmann and Soomere, 2013; Soomere et al., 2014), on the German coast (Chrastansky and Callies, 2009), in the Mediterranean Sea (Olita et al., 2012; Alves et al., 2015; Jiménez Madrid et al., 2016; Liubartseva et al., 2016) and are currently used worldwide (Pradhan et al., 2022; Abdallah and Chantsev, 2022; Sbragio and Martins, 2022). Backward-in-time approach was adopted in atmospheric science to identify the source of a pollutant or emissions from potential sites (Flesch et al.,1995; Lin et al.,

2003; Seibert and Frank, 2004; Stohl et al., 2012) and, in the ocean, the drift of marine organisms (Batchelder, 2006; Barry et al., 2023), the sources of SAR detected oil spills (Vespe et al., 2011, Perkovic et al. 2016; Zodiatis et al., 2017b), and for oil spill risk analysis (Ciappa and Costabile, 2014; Suneel et al., 2016; Ciappa, 2021). Oil transport in the Mediterranean Sea was investigated in the Adriatic Sea (Liubartseva et al., 2014), in the Levantine basin (Alves et al., 2015), and in the whole basin (Jiménez Madrid et al., 2016), providing results that are confirmed here. The results of this study indicate that in the Mediterranean Sea, on average, oil transport is more predictable in summer, when it is dominated by the current, and winter oil spills can reach far locations pushed by the wind. However, at local scale, oil trajectory analysis is necessary to understand the combined effects of local winds and surface currents. Oil trajectories are due to the time-cumulated action of winds and surface current. While oil trajectories are similar in the Sicily Channel (Fig. 9f) or in the Aegean Sea (Fig. 10c) in summer due to the steady surface current pattern and the northern Etesian wind, respectively, providing a clear indication of where oil spills should be looked for, winds and surface currents are variable around most Mediterranean coastal sites, and the most likely direction of provenience of the oil spills unknown. Oil trajectories analysis addresses complex – and crucial for marine protected areas - cases such as these.

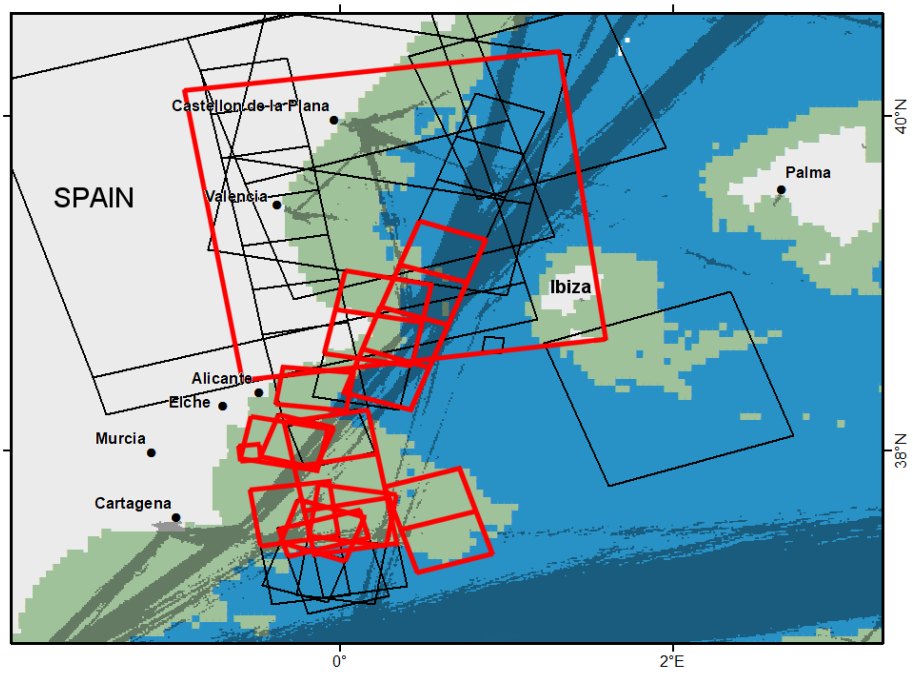

Fig. 12. COSMO-SkyMed X-SAR scenes available on 15 August 2022 over the Spanish coast and Balearics. The area of > 5% beaching probability in August is shown in green, the main tanker routes in background (grey). The estimate of the high priority scenes is shown in red.

It's worth mentioning that oil trajectories analysis is not designed to predict where a real oil spill will beach *after* being detected by SAR. In this case, the best prediction is obtained running an oil spill model forward-in-time, where the type of the oil

(usually known) is assigned and the simulation is driven by wind and current forecasts of the following days (a list of operational forecasting systems in the Mediterranean Sea is provided in Zodiatis et al., 2017a). Rather, oil trajectory analysis aims to identify, *before* the acquisition of any new SAR image, where to collect more images to improve the safeguarding of marine protected areas. This would mean changing the very premise of the acquisition strategy, from monitoring sea areas where oil spills are most likely to occur to sea areas where oil spills are most dangerous for the marine environment. As an example, Fig. 12 shows the scenes that can be tasked for one SAR constellation (COSMO-SkyMed) in one day (15 August 2022) over the Spanish coast. This example gives a measure of the large number of scenes that are already acquirable today when several SAR constellations are taken into account. In August (Fig. 12), the higher-than-5% beaching probability area is extended offshore between Alicante and Cartagena, and the area is crossed by tanker routes. A proposal for high priority scenes thus to be selected in summer for oil spill surveillance is shown in red. Not included are scenes over the tanker route west of Balearics, as oil spills occurring there are unlikely to reach the islands in summer, and the scene SE of Ibiza, as the area is not crossed by tankers.

5 - Conclusions

Results of oil trajectory analysis provide information on point of beaching, probability, and time it will take to reach the coast. The analysis, extended to the marine protected areas of the Mediterranean Sea, provides information on where to focus oil spill surveillance, most especially by satellites, which cover large areas. Frequent surveillance is a deterrent to cleaning operations of gas and oil tankers in open waters, which result in illegal discharge of oil.

The oil trajectory analysis in the Mediterranean Sea shows a marked seasonal signal, with similar winter (November - March) and summer (May - September) patterns. Oil transport in winter is faster and less predictable than in summer, due to wind advection prevailing over current advection. The results show that the beaching probability, i.e., the probability than an oil spill will reach the coast, is 25% at 5 km, 10% at 10 km, 5% at 15 km. A guess threshold of 5% of beaching probability in marine protected areas was adopted to decide if a sea area merits monitoring priority. Another key element is the intersection with the main oil tanker routes, which is where oil spills occur most often. In 5 major areas of the Mediterranean Sea, specific sea areas deserving consideration have been identified in summer and winter months.

This paper aims to introduce priority criteria of oil spill monitoring based on the results of the oil trajectory analysis in the Mediterranean Sea. An automated oil spill detection system in Mediterranean Sea is described in Yang et al. (2022) and is based on Sentinel-1 SAR imagery and a trained deep learning object detector to detect oil spills. In the near future, when a large dataset of SAR imagery will be available, SAR tasking could be supported by the results of oil trajectory analysis to decide where and when to acquire more data. A future satellite oil spill monitoring system that includes results of oil trajectory

analysis would prioritize the tasking of new SAR acquisitions over offshore marine protected areas on a monthly basis, changing the acquisition plan month by month. SAR images over these areas could be tasked, acquired, and processed before those over other offshore areas.

Acknowledgements

This study is based on physical data provided by Copernicus Marine Environmental Service (CMEMS), AIS data provided by the European Marine Observation and Data Network (EMODnet), MPA data provided by the MArine Protected Areas in the MEDiterranean (MAPAMED) database, Copernicus Sentinel-1 scenes provided by the European Space Agency (ESA). All these organizations providing an easy access to the data are acknowledged. Thanks to the Editor and two anonymous referees for improvements of the original manuscript. A special thanks to Elena Cantoni for revising the text.

Appendix A - monthly mean kinetic energy

The kinetic energy maps of current and of the wind component of oil transport (3% of wind speed) are reported in Fig. S1. Kinetic energy is exhaustive for the identification of known winds and currents, and main currents and winds are summarized in Table 3 (the related literature can be found in Millot (1999), Millot and Taupier-Letage (2005), and Pinardi and Masetti (2000)). Kinetic energy is not always exhaustive in attributing oil transport to current or to wind advection. Indeed, high kinetic energy can be found where strong but variable winds and currents cause looping trajectories which do not overly affect oil transport, and low kinetic energy can be found where weak but stable winds and currents affect the oil transport patterns.

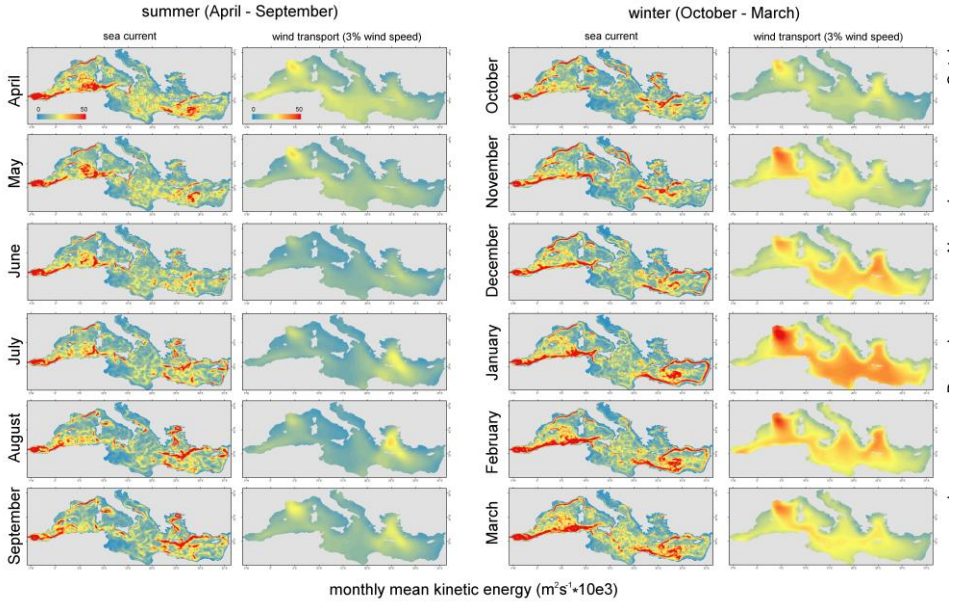

Fig. S1. Monthly kinetic energy in summer and winter of the sea surface current and of the wind component of the oil transport (3% of wind speed), averages over the period 2015 - 2019.

Table 3 – Monthly occurrence of main current systems and winds of the Mediterranean Sea. The North Current (NC) flowing along the northern coast of Western Mediterranean is also called Liguro-Provençal current.

	Summer						winter					
Main currents	Apr	May	Jun	Jul	Aug	Sep	Oct	Nov	Dec	Jan	Feb	Mar
Alboran Gyres	x	x	x	x	x	x	x	x	x	x	x	x
Balearic Current	x	x	x	x	x	x	x	x	x	x	x	x
North Current (NC)	x	x	x	x	x	x	x	x	x	x	x	x
Algerian Current (AC)	x	x	x	x				x	x	x	x	x
Atlantic Ionian Stream (AIS)		x	x	x	x	x						
Libyo-Egyptian Current					x	x	x	x	x	x	x	x
Ligurian Gyre					x	x	x	x	x	x	x	x
Asia Minor Current (AMC)	x			x	x	x			x	x	x	x
Western Adriatic Current (WAC)					x	x	x	x	x			
Main winds												
Mistral								x	x	x	x	x
Etesian (meltemi)				x	x	x	x	x	x	x	x	x
North Adriatic bora	x						x	x	x	x	x	x

6 – References

Abascal, A.J., Castanedo, S., Fernández, V. *et al.* 2012. Backtracking drifting objects using surface currents from high-frequency (HF) radar technology. *Ocean Dynamics* **62**, 1073–1089. https://doi.org/10.1007/s10236-012-0546-4

Abdallah M.I, Chantsev V., 2022. Modeling marine oil spill trajectory and fate off Hurghada, Red Sea coast, Egypt, Egyptian Journal of Aquatic Biology and Fisheries, Volume 26, Issue 6, Page 41-61, DOI: 10.21608/ejabf.2022.269676

Alves, T.M.; Kokinou, E.; Zodiatis, G.; Lardner, R.; Panagiotakis, C.; Radhakrishnan, H., 2015. Modelling of oil spills in confined maritime basins: The case for early response in the Eastern Mediterranean Sea. Environ. Pollut., 206, 390–399. https://doi.org/10.1016/j.envpol.2015.07.042.

ASCE Task Committee on Modeling Oil Spills, 1996. State-of-the-art review of modeling transport and fate oil spills. J. Hydraulic Eng. 122 (11), 594–609. https://doi.org/10.1061/(ASCE)0733-9429(1996)122:11(594)

Astraldi, M., Gasparini, G.P., Sparnocchia, S., Moretti, M., Sansone, E., 1996. The characteristics of water masses and the water transport in the Sicily Strait at long timescales. Bulletin de l'Institut Océanographique (Monaco) 17, 95–115.

Astraldi, M., Gasparini, G.P., Sparnocchia, S., 1998. Water masses and seasonal hydrographic conditions in the Sardinia–Sicily–Tunisia region. Rapport de la Commission Internationale de la Mer Méditerranée 35, 1998.

Azorin-Molina, C., D. Chen, S. Tijm, and M. Baldi, 2011. A multi-year study of sea breezes in a Mediterranean coastal site: Alicante (Spain). *Int. J. Climatol.*, **31**, 468–486, doi:10.1002/joc.2064.

Barry P.J., C. Beraud, L.E. Wood, H.J. Tidbury, 2023. Modelling of marine debris pathways into UK waters: Example of non-native crustaceans transported across the Atlantic Ocean on floating marine debris, Marine Pollution Bulletin, Volume 186, 114388, https://doi.org/10.1016/j.marpolbul.2022.114388.

Batchelder, H.P., 2006. Forward-in-time-/backward-in-time-trajectory (FITT/BITT) modeling of particles and organisms in the coastal ocean. J. Atmos. Oceanic Technol. 23 (5), 727–741. https://doi.org/10.1175/JTECH1874.1

Carpenter, A., 2016. European Maritime Safety Agency Activities in the Mediterranean Sea. In: Carpenter, A., Kostianoy, A. (eds) Oil Pollution in the Mediterranean Sea: Part I. The Handbook of Environmental Chemistry, vol 83. Springer, Cham. https://doi.org/10.1007/698_2016_18

Carpenter, A., Donner, P., Johansson, T., 2017. The Role of REMPEC in Prevention of and Response to Pollution from Ships in the Mediterranean Sea. In: Carpenter, A., Kostianoy, A. (eds) Oil Pollution in the Mediterranean

Sea: Part I. The Handbook of Environmental Chemistry, vol 83. Springer, Cham. https://doi.org/10.1007/698_2017_169
Chen H., 2019. Performance of a simple backtracking method for marine oil source searching in a 3D ocean, Marine Pollution Bulletin, Volume 142, Pages 321-334, ISSN 0025-326X, https://doi.org/10.1016/j.marpolbul.2019.03.045.
Chrastansky, A., Callies, U., 2009. Model-based long-term reconstruction of weather driven variations of chronic oil pollution along the German North Sea coast. Mar. Pollut. Bull. 58, 967–975. https://doi.org/10.1016/j.marpolbul.2009.03.009.
Ciappa A. and S. Costabile, 2014. Oil spill hazard assessment using a reverse trajectory method for the Egadi marine protected area (Central Mediterranean Sea), Marine Pollution Bulletin, Volume 84, Issues 1, Pages 44-55, https://doi.org/10.1016/j.marpolbul.2014.05.044.
Ciappa, A.C., 2021. Reverse trajectory study of oil spill risk in Cyclades Islands of the Aegean Sea, Regional Studies in Marine Science, Volume 41, ISSN 2352-4855, https://doi.org/10.1016/j.rsma.2020.101580.
De Dominicis M., D. Bruciaferri, R. Gerin, N. Pinardi, P.M. Poulain, P. Garreau, G. Zodiatis, L. Perivoliotis, L. Fazioli, R. Sorgente, C. Manganiello, 2016. A multi-model assessment of the impact of currents, waves and wind in modelling surface drifters and oil spill. *Deep Sea Research Part II: Topical Studies in Oceanography*, 2016, 133: 21-38, https://doi.org/10.1016/j.dsr2.2016.04.002.
Delpeche-Ellmann, N.C., Soomere, T., 2013. Investigating the Marine Protected Areas most at risk of current-driven pollution in the Gulf of Finland, the Baltic Sea, using a Lagrangian transport model. Mar. Pollut. Bull. 67 (1–2), 121–129. https://doi.org/10.1016/j.marpolbul.2012.11.025.
Escudier, R., Clementi, E., Omar, M., Cipollone, A., Pistoia, J., Aydogdu, A., Drudi, M., Grandi, A., Lyubartsev, V., Lecci, R., Cretí, S., Masina, S., Coppini, G., & Pinardi, N., 2020. Mediterranean Sea Physical Reanalysis (CMEMS MED-Currents) (Version 1) Data set. Copernicus Monitoring Environment Marine Service (CMEMS). https://doi.org/10.25423/CMCC/MEDSEA_MULTIYEAR_PHY_006_004_E3R1
Fingas, M.F., 2011. Introduction to Spill Modeling. Editor(s): Mervin Fingas, Oil Spill Science and Technology, Gulf Professional Publishing, Pages 187-200, https://doi.org/10.1016/B978-1-85617-943-0.10008-5.
Flesch, T.K., Wilson, J.D., Yee E., 1995. Backward-time Lagrangian stochastic dispersion models and their application to estimate gaseous emissions. J. Appl. Meteor. 34, 1320–1332. https://doi.org/10.1175/1520-0450(1995)034<1320:BTLSDM>2.0.CO;2
Galt, J.A., Payton, D.L., 1983. The use of receptor mode trajectory analysis techniques for contingency planning. In: International Oil Spill Conference Proceedings: February 1983, vol. 1983, no. 1, pp. 307–311. https://doi.org/10.7901/2169-3358-1983-1-307
García, E., Tintor_e, J., Pinot, J.M., Font, J., Manriquez, M., 1994. Surface circulation and dynamics of the Balearic sea. In: Seasonal and Interannual Variability of the Western Mediterranean Sea. American Geophysical Union, pp. 73e91. http://dx.doi.org/10.1029/CE046p0073.
Janeiro J., A. Neves, F. Martins, P. Relvas, 2017. Integrating technologies for oil spill response in the SW Iberian coast, Journal of Marine Systems, Volume 173, Pages 31-42, ISSN 0924-7963, https://doi.org/10.1016/j.jmarsys.2017.04.005.
Jiménez Madrid, J. A., Garcìa-Ladona, E., and Blanco-Meruelo, B., 2016. Oil spill beaching probability for the Mediterranean Sea, in *Oil Pollution in the Mediterranean Sea: Part I. The Handbook of Environmental Chemistry*, Vol. 83, eds A. Carpenter and A. Kostianoy (Cham: Springer), doi: 10.1007/698-2016-37
Lin, J.C., Gerbig, C., Wofsy, S.C., Andrews, A.E., Daube, B.C., Davis, K.J., Grainger, C.A., 2003. A near-field tool for simulating the upstream influence of atmospheric observations: the Stochastic Time-Inverted Lagrangian Transport (STILT) model. J. Geophys. Res. 108, 4493. http://dx.doi.org/10.1029/2002JD003161.
Liubartseva S., M. De Dominicis, P. Oddo, G. Coppini, N. Pinardi, N. Greggio, 2014. Oil spill hazard from dispersal of oil along shipping lanes in the Southern Adriatic and Northern Ionian Seas, Marine Pollution Bulletin, Volume 90, Pages 259-272, https://doi.org/10.1016/j.marpolbul.2014.10.039.
Liubartseva, S., Coppini, G., Pinardi, N., De Dominicis, M., Lecci, R., Turrisi, G., Cretì, S., Martinelli, S., Agostini, P., Marra, P., and Palermo, F., 2016. Decision support system for emergency management of oil spill accidents in the Mediterranean Sea, Nat. Hazards Earth Syst. Sci., 16, 2009–2020, https://doi.org/10.5194/nhess-16-2009-2016.

Liubartseva S., M. Smaoui, G. Coppini, G. Gonzalez, R. Lecci, S. Cretì, I. Federico, 2020. Model-based reconstruction of the Ulysse-Virginia oil spill, October-November 2018, Marine Pollution Bulletin, Volume 154, 2020, 111002,ISSN 0025-326X, https://doi.org/10.1016/j.marpolbul.2020.111002.
Lu, X., Soomere, T., Stanev, E.V., Murawski, J., 2012. Event driven approach for the identification of the environmentally safe fairway in the south-western Baltic Sea and Kattegat. Ocean Dyn. 62, 815–829. Doi: 10.1007/s10236-012-0532-x
Millot, C., 1999. Circulation in the Western Mediterranean Sea, Journal of Marine Systems,Volume 20, Issues 1, Pages 423-442, ISSN 0924-7963, https://doi.org/10.1016/S0924-7963(98)00078-5.
Millot, C., Taupier-Letage, I., 2005. Circulation in the Mediterranean Sea. In: Saliot, A. (eds) The Mediterranean Sea. Handbook of Environmental Chemistry, vol 5K. Springer, Berlin, Heidelberg. https://doi.org/10.1007/b107143
Murawski, J., Woge Nielsen, J., 2013. Applications of an oil drift and fate model for fairway design. In: Soomere, T., Quak, E. (Eds.), Preventive Methods for Coastal Protection. Springer, Cham, pp. 367–415. DOI: 10.1007/978-3-319-00440-2_11
Olita, A., Cucco, A., Simeone, S., Ribotti, A., Fazioli, L., Sorgente, B., Sorgente, R., 2012. Oil spill hazard and risk assessment for the shorelines of a Mediterranean coastal archipelago. Ocean Coast. Manag. 57, 44–52, https://doi.org/10.1016/j.ocecoaman.2011.11.006.
Perkovic, M., Harsch, R., Ferraro, G., 2016. Oil Spills in the Adriatic Sea. In: Carpenter, A., Kostianoy, A. (eds) Oil Pollution in the Mediterranean Sea: Part II. The Handbook of Environmental Chemistry, vol 84. Springer, Cham. https://doi.org/10.1007/698_2016_53
Pinardi N., Masetti E. 2000. Variability of the large scale general circulation of the Mediterranean Sea from observations and modelling: a review. Palaeogeogr Palaeoclimatol Palaeoecol. 15:153–173. doi: 10.1016/S0031-0182(00)00048-1
Polinov, S., R. Bookman, and N. Levin. 2021. "Spatial and Temporal Assessment of Oil Spills in the Mediterranean Sea." *Marine Pollution Bulletin* 167: 112338. doi: 10.1016/j.marpolbul.2021.112338.
Pradhan, B., Das, M. & Pradhan, C., 2022. Trajectory modelling for hypothetical oil spill in Odisha offshore, India. *J Earth Syst Sci* 131, 205 (2022). https://doi.org/10.1007/s12040-022-01946-6
Robinson, A.J., Sellshop, J., Warn-Warnas, A., Leslie, W.J., Lozano, C.J., Halley Jr., P.J., Anderson, L.A., Lermusiaux, P.F.J., 1999. The Atlantic Ionian Stream. J. Mar. Syst. 20, 129–156. https://doi.org/10.1016/S0924-7963(98)00079-7.
Sbragio R., M. R. Martins, 2022. Modelling and CFD simulation of the trajectory of an oil spill in a large domain: Analysis of the 2003 Foss Barge - Point Wells event, Ocean Engineering, Volume 262, https://doi.org/10.1016/j.oceaneng.2022.112315.
Seibert, P., Frank, A., 2004. Source-receptor matrix calculation with a Lagrangian particle dispersion model in backward mode. Atmos. Chem. Phys. 4, 51–63. https://doi.org/10.5194/acp-4-51-200
Soomere, T., Viikmäe, B., Delpeche, N., Myrberg, K., 2010. Towards identification of areas of reduced risk in the Gulf of Finland, the Baltic Sea. Proc. Estonian Acad. Sci. 59 (2), 156–165. doi: 10.3176/proc.2010.2.15
Soomere, T., Döös, K., Lehmann, A., Markus Meier, H.E., Murawski, J., Myrberg, K., Stanev, E., 2014. The potential of current- and wind-driven transport for environmental management of the Baltic Sea. AMBIO 43, 94–104. http:// dx.doi.org/10.1007/s13280-013-0486-.
Soussi A. *et al*., 2019. An oil spill trajectory model: validation in the Mediterranean Sea, *2019 International Symposium on Systems Engineering (ISSE)*, 2019, pp. 1-6, doi: 10.1109/ISSE46696.2019.8984542.
Stohl, A., Seibert, P., Wotawa, G., Arnold, D., Burkhart, J.F., Eckhardt, S., Tapia, C., Vargas, A., Yasunari, T.J., 2012. Xenon-133 and caesium-137 releases into the atmosphere from the Fukushima Dai-ichi nuclear power plant: determination of source term, atmospheric dispersion, and deposition. Atmos. Chem. Phys. 12, 2313–2343. https://doi.org/10.5194/acp-12-2313-2012
Suneel V., A. Ciappa, P. Vethamony, 2016. Backtrack modeling to locate the origin of tar balls depositing along the west coast of India, Science of The Total Environment, Volumes 569-570, Pages 31-39, https://doi.org/10.1016/j.scitotenv.2016.06.101.
Thyng K. M., 2019. Deepwater Horizon Oil could have naturally reached Texas beaches, Marine Pollution Bulletin, Volume 149, 110527, ISSN 0025-326X, https://doi.org/10.1016/j.marpolbul.2019.110527.

Thomson, D., 1987. Criteria for the selection of stochastic models of particle trajectories in turbulent flows. *Journal of Fluid Mechanics, 180*, 529-556. doi:10.1017/S0022112087001940

Torgrimson, G.M., 1981. A comprehensive model for oil spill simulation. In: Proceedings of the Oil Spill Conference. American Petroleum Institute,Washington DC, pp. 423–428.https://doi.org/10.7901/2169-3358-1981-1-423

Vespe M., G. Ferraro, M. Posada, H. Greidanus and M. Perkovic, 2011. Oil spill detection using COSMO-SkyMed over the adriatic sea: The operational potential, *2011 IEEE International Geoscience and Remote Sensing Symposium*, 2011, pp. 4403-4406, doi:10.1109/IGARSS.2011.6050208

Viikmäe, B., Torsvik, T., Soomere, T., 2013. Impact of horizontal eddy diffusivity on Lagrangian statistics for coastal pollution from a major marine fairway. Ocean Dyn. 63 (5), 589–597. https://doi.org/10.1007/s10236-013-0615-3

Yang, Y.-J., Singha, S., and Goldman, R., 2022. An automatic oil spill detection and early warning system in the Southeastern Mediterranean Sea, EGU General Assembly 2022, Vienna, Austria, 23–27 May 2022, EGU22-8408, https://doi.org/10.5194/egusphere-egu22-8408, 2022.

Zodiatis, G. *et al.*, 2017a. Numerical Modeling of Oil Pollution in the Eastern Mediterranean Sea. In: Carpenter, A., Kostianoy, A. (eds) Oil Pollution in the Mediterranean Sea: Part I. The Handbook of Environmental Chemistry, vol 83. Springer, Cham. https://doi.org/10.1007/698_2017_131

Zodiatis, G., Lardner, R., Alves, T. M., Krestenitis, Y., Perivoliotis, L., Sofianos, S., & Spanoudaki, K., 2017b. *Oil spill forecasting (prediction). Journal of Marine Research, 75(6), 923–953.* doi:10.1357/002224017823523982